Journal of Power Sources 240 (2013) 417–420

Contents lists available at SciVerse ScienceDirect

Journal of Power Sources

journal homepage: www.elsevier.com/locate/jpowsour

Short communication

Feasibility study of hydrogen/iron redox flow cell for grid-storage applications

M. Alon [a], A. Blum [b], E. Peled [a,*]

[a] School of Chemistry, Tel Aviv University, POB 39040, Tel Aviv 69978, Israel
[b] EnStorage Inc., POB 199, Moshav Hazav, Israel

HIGHLIGHTS

- Hydrogen/iron regenerative fuel cell was tested for the first time and showed stable cycle life.
- Electrolytes prepared using different iron salts exhibited different behavior.
- Peak power density was registered at 0.27 W cm^{-2}.
- Energy conversion of up to 82% was achieved.

ARTICLE INFO

Article history:
Received 28 November 2012
Received in revised form
6 March 2013
Accepted 7 April 2013
Available online 18 April 2013

Keywords:
Hydrogen
Flow batteries
Regenerative fuel cells
Energy-storage

ABSTRACT

In this study, the hydrogen/iron redox flow cell was evaluated in order to estimate its potential as an energy-storage system. The system was studied for the first time, for energy-storage applications, with electrolytes composed of several different iron salts and their conjugate acids. Cell performance varied with electrolyte composition. Best results were obtained with a solution of iron sulfate in sulfuric acid: stable performance, good capacity utilization, energy-conversion efficiency of up to 82% and a power density of up to 0.27 W cm^{-2}, with no optimization of cell components. The results show the potential of the hydrogen/iron system as a candidate for energy-storage and further optimization should greatly enhance performance.

1. Introduction

The depletion of existing energy sources and the rapid increase in the consumption of electricity have led, in recent years, to extensive research on large-scale energy-storage systems. The main uses of these systems include the integration of renewable energy from solar and wind sources and peak leveling by storing power generated during periods of low consumption, and releasing it during peak demand, thus increasing power-generation efficiency and minimizing the need for expensive back-up power generators. New technologies have the potential of becoming a dominant component in energy distribution, such as redox flow batteries (RFB) and regenerative fuel cells (RFC), superconducting magnetic energy storage (SMES) and double-layer capacitors (EDLC) [1]. RFBs and RFCs enable the storing and release of electrical energy by means of chemical species undergoing electrochemical reactions. These chemical species are stored outside the electrochemical cell, enabling the differentiation between stored energy and the rated power, leading to flexible operation compatible with a large number of applications. A typical flow cell consists of two non-consumed electrodes, made of high-surface-area carbon and a separating membrane with selective ion conductivity [2,3]. Extensive research of redox cells is being carried out in an attempt to achieve a reliable and stable system, with long cyclability at an acceptable cost. A few of the most researched redox systems include the vanadium redox battery (VRB), and the iron/chromium and zinc/bromine flow batteries. The iron/chromium system was first developed in 1974 by the American National Aeronautics and Space Administration (NASA) [4,5]. In this system, the cathode electrolyte is composed of Fe(III) ions which undergo reduction while the Cr(II) ions at the anode are oxidized, with most systems using hydrochloric acid as the supporting electrolyte [3]. One challenge of this system is minimizing hydrogen evolution at the

* Corresponding author. Tel.: +972 3 640 8438.
E-mail addresses: alonmeit@tau.ac.il (M. Alon), arnon.blum@enstorageinc.com (A. Blum), peled@tau.ac.il (E. Peled).

0378-7753/$ – see front matter © 2013 Elsevier B.V. All rights reserved.
http://dx.doi.org/10.1016/j.jpowsour.2013.04.032

chromium electrode during charge, which leads to a decrease in coulombic efficiency and presents the need for a rebalance cell. The vanadium flow battery is one of the most-studied redox systems [6–9]. Since this system uses the same electrolyte on both sides of the cell, it does not suffer from electrolyte degradation following ion transfer. This system is considered to be highly efficient, though presents high sensitivity of system cost to purity of vanadium [10]. Zinc/bromine is another extensively studied system [11–14]. It is considered a hybrid flow battery in which metallic zinc is deposited directly on the anode during the charging process. The zinc is reoxidized during discharge, while bromine is reduced to bromide at the cathode.

In the hydrogen/iron redox flow cell (which is also a regenerative fuel cell) the overall reaction taking place is $½H_2 + Fe^{+3} \leftrightarrow H^+ + Fe^{+2}$, $E^0 = 0.770$ V. Advantages of the system include no capacity loss by mixing of cathodic and anodic materials (through the process of reactant recovery) and the use of inexpensive and widely available active materials. The use of hydrogen gas with the Fe(III)/Fe(II) redox couple was examined in a fuel-cell system (discharge only) by Fatih et al. [15], in a single cell with low platinum loading for hydrogen oxidation, carbon felt for iron reduction and a Nafion membrane. In their work, a solution of ferric ammonium sulfate, ferrous sulfate and sulfuric acid was used, with 0.9 M total iron concentration at an Fe(III)/Fe(II) ratio of 9 and at pH 1. The best results show a maximal energy density of 0.17 W cm^{-2}, at 70 °C.

The charge-transfer process in the Fe(III)/Fe(II) redox couple is an inner-sphere process [16]; therefore, the charge-transfer kinetics is highly dependent on the nature of the solute iron complex and its electrochemical and physical characteristics. In the presence of different ligands, Fe(III) and Fe(II) ions can take the form of free ions or different complexes in the solution, thus presenting a considerable challenge in the choice of the optimal electrolyte composition and the optimal operating conditions for each composition. In this work, electrolytes containing different iron salts and their conjugate acids were used to evaluate cell performance. Results revealed high efficiencies, good power density, high capacity utilization and good stability and cyclability.

2. Experimental

All electrochemical evaluations were made on a single cell with an active area of 7 cm^2, as described elsewhere [17]. The cell is composed of graphite flow fields, in interdigit form (flow-through) on the iron side and serpentine (flow-by) on the hydrogen side, with copper current-collector end plates. The hydrogen electrode was fabricated by applying a gas-diffusion layer (GDL) consisting of a mixture of 25% (w/w) PVdF (Kynar) and Vulcan XC-72R on top of a carbon cloth (Ballard) by the doctor-blade method. The catalyst ink consisting of a catalyst powder (PtIr alloy on Vulcan XC-72), 25% (w/w) Nafion (5% in alcohol/water, Aldrich) and isopropanol, was coated with the use of doctor-blade on the previously deposited GDL. Both layers underwent curing and acid treatment (0.5 M H_2SO_4, 80 °C, 1 h). The process resulted in sublayer loading of about 4 mg cm^{-2} carbon and catalytic loading of 1 mg PtIr cm^{-2}. The iron electrode was fabricated by applying a microporous catalytic layer consisting of a mixture of 10% PVdF (Kynar), MCMB (Osakagas) and catalyst powder (PtIr alloy on Vulcan XC-72) on carbon paper (20% PTFE, Toray) by the doctor-blade method. The layers underwent curing and acid treatment. The process resulted in electrode loading of 2 mg cm^{-2} carbon and metal loading of 0.06 mg PtIr cm^{-2}. A 160 μm nano-porous proton-conducting membrane (NP-PCM) [18] was used. The membrane electrode assembly (MEA) was hot-pressed at 100 °C. Four electrolyte solutions were prepared with DI water by the use of: $Fe_2(SO_4)_3 \cdot 7H_2O$ (analytical, Sigma) and H_2SO_4 (96%, Sigma), $FeCl_3$ (analytical, Merck) and HCl (32%, Bio Lab) and lastly Fe_2O_3 (analytical, Sigma) and HBr (48%, Sigma). Electrolyte compositions are shown in Table 1, with the different solutions represented by the iron salt they contain. Hydrogen was generated with the use of an electrolyzer, and hydrogen pressure build-up was controlled by the adjustment of a needle valve placed at the gas exit from the cell. The overpotential developed on the iron electrode was measured with the use of a small piece of carbon paper, coated with a porous GDL layer consisting of 4 mg cm^{-2} XC-72 carbon (0.25 cm^2), submerged in the electrolyte solution tank, near the outlet stream, and connected to a Pt wire (Fe(III)/Fe(II) reference electrode). The voltage was measured between the iron half-cell and the iron reference electrode, expressing the activation, concentration and the ohmic overpotentials developed at the iron electrode. The cells were examined with a Maccor battery-test system, in a polarization procedure to evaluate peak power density and limiting currents. Measurements were made at current densities of up to 0.64 A cm^{-2} which was the maximal current density of the battery-test analyzer channel. Voltage measurements were taken after 30 s at any given current density step, in order to ensure voltage stabilization. Performance was evaluated in a cycle-life procedure of charge and discharge cycles at constant current density, in order to estimate the efficiency, capacity utilization and stability. Hydrogen flow was set at 15–20 ml min^{-1} at 1 atm gauge pressure. A 20–22 ml of electrolyte solution was circulated through the cell at a flow rate of 18 ml min^{-1}.

Table 1
Electrolyte compositions, in fully charged and fully discharged states.

Electrolyte code	Comp. fully charged [M]	Comp. fully discharged [M]
1.5 M $FeCl_3$	1.5 $FeCl_3$; 2 HCl	1.5 $FeCl_2$; 3.5 HCl
1.4 M $FeBr_3$	1.4 $FeBr_3$; 2 HBr	1.4 $FeBr_2$; 3.4 HBr
1 M $FeSO_4$	0.5 $Fe_2(SO_4)_3$; 2 H_2SO_4	1 $FeSO_4$; 2.5 H_2SO_4
1.5 M $FeSO_4$	0.75 $Fe_2(SO_4)_3$; 2 H_2SO_4	1.5 $FeSO_4$; 2.75 H_2SO_4

3. Results and discussion

3.1. Polarization measurements

Cell polarization was measured for all systems at 40 °C. Electrolyte solutions were charged to 0.85–0.9 V before polarization (Fig. 1). Most systems showed good power densities, the highest,

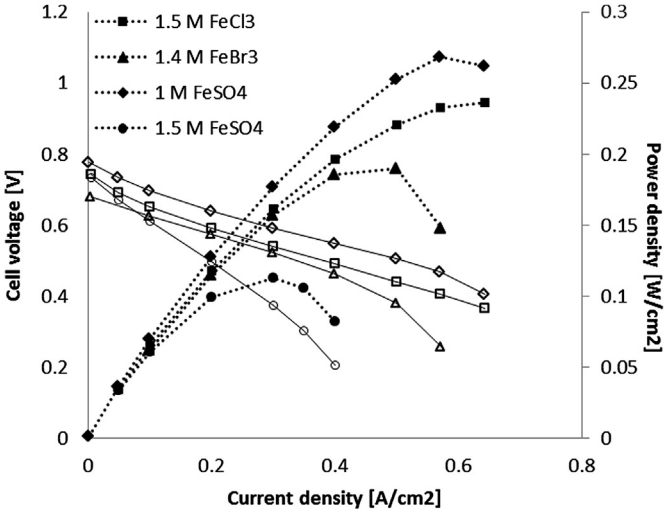

Fig. 1. Polarization curves for different iron electrolytes, taken at 40 °C. Full marks represent power density, hollow marks represent voltage.

0.27 W cm^{-2}, was obtained for the 1 M $FeSO_4$ electrolyte. A similar electrolyte with an iron concentration of 1.5 M had a low power density – only 0.11 W cm^{-2}. The $FeCl_3$ electrolyte had a high value of 0.24 W cm^{-2} at the highest current density possible with the equipment used. A lower power density of 0.19 W cm^{-2} was measured with the use of the $FeBr_3$ electrolyte. Measurements of the overpotential developed on the iron electrode, in all electrolytes, exhibited very low values, of 5–20 mV at 0.64 A cm^{-2}, out of a total of up to 300 mV cell overpotential. This indicates that the reduction of Fe(III) to Fe(II) has fast kinetics and is less affected by the ligand on the iron ions. The high polarization is therefore attributed to hydrogen oxidation at the hydrogen electrode. Since crossover of electrolyte solution to the hydrogen electrode was observed in the cycle-life measurements (Section 3.2), the difference in peak power densities, for the different electrolytes, may be the result of the variations of the kinetics of hydrogen oxidation in different environments. Adsorption of species on the catalytic layer of the hydrogen electrode may affect charge-transfer processes and lower the number of available catalytic sites, giving rise to a lower exchange-current density. The coverage of chloride and bromide on the Pt(111) surface was reported, for electrolyte solutions of 0.01 M KCl or KBr, in a supporting electrolyte of 0.1 M $HClO_4$ [19]. This work showed coverage of 0.4 and 0.43 for chloride and bromide, respectively, at a voltage of 0.03 V vs SHE and increasing coverage at higher potentials. During discharge of the hydrogen/iron cell, the voltage on the hydrogen electrode shifts to positive values, increasing with the increase in current density. Therefore, adsorption of halides from the electrolyte solution may occur, which could lead to slower kinetics and a lower power density. On the other hand, sulfuric acid is considered to be inactive on a platinum surface in the hydrogen redox voltage region, and may begin adsorption of bisulfate ions (or sulfate, depending on pH) at potentials higher than 0.3 V vs RHE [20]. Cyclic-voltammetry measurements were used to measure the activity of polycrystalline platinum in sulfuric acid solutions with and without the addition of HBr and in 3 M HBr [21]. In 3 M HBr the charge related to Pt–H desorption dropped by up to 50% relative to the charge obtained in 0.5 M sulfuric acid, an effect caused by irreversible adsorption of bromide. This was followed by a reduction in the hydrogen exchange-current density. These findings are in agreement with the lower power measured for the $FeCl_3$ and $FeBr_3$ cells.

3.2. Cycle-life measurements

Cycle-life was measured under constant current conditions for the 1.5 M $FeCl_3$ electrolyte and 1 M and 1.5 M $FeSO_4$ electrolytes. Operating conditions were set at 0.1 A cm^{-2} current density, 0.4 V discharge limiting voltage, 0.8 V charge limiting voltage for the 1.5 M $FeCl_3$ and $FeSO_4$ electrolytes and 0.85 V for the 1 M $FeSO_4$ electrolyte. The coulombic efficiency (QE) was determined by the ratio between discharge and charge capacities and the energy-conversion efficiency (EE) by the ratio between discharge and charge energies. The voltage efficiency (VE) was calculated by dividing the measured energy-conversion efficiency by the coulombic efficiency. Capacity, efficiency and cycle-life results are given in Fig. 2 and Table 2. The cells exhibit good stability with all electrolytes, indicating reversibility of the redox reactions and stability of the hydrogen-electrode catalyst, under the chosen operating conditions, in the examined time frame. Though extended durability was not examined, some cells operated for more than 200 cycles. The $FeCl_3$ electrolyte showed a capacity utilization of up to 90% (0.72 Ah out of a theoretical 0.8 Ah), with efficiencies of 91% QE and 74% EE. The results obtained with the 1 M $FeSO_4$ electrolyte reveal high efficiencies, with 97% QE, 84% VE and 82% EE. The high QE with 1 M $FeSO_4$ electrolyte indicates low

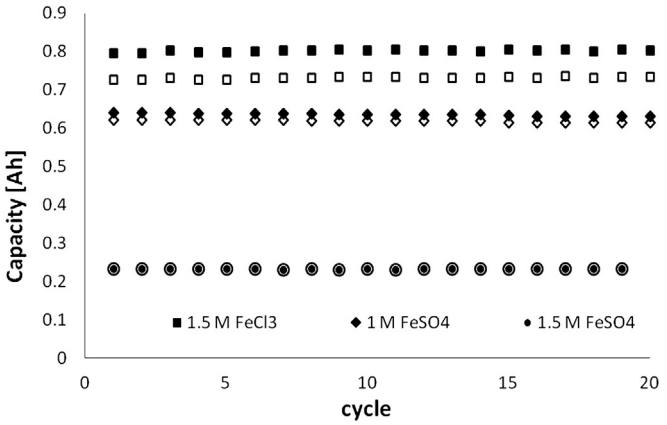

Fig. 2. Capacity charts vs. cycle number, for different iron electrolytes, taken at 0.1 A cm^{-2} and 60–65 °C. Charge capacity is represented by full marks, discharge capacity is represented by hollow marks.

crossover of Fe(III) to the hydrogen electrode. Relative to 1.5 M $FeCl_3$ electrolyte, higher QE may be the result of lower Fe(III) concentration and may also suggest slower transfer processes of Fe(III) ions through the membrane, in the $FeSO_4$ solution.

Increasing the iron concentration in the $FeSO_4$ electrolyte, from 1 M to 1.5 M resulted in lower capacities, under 30% of the total theoretical capacity, with high overpotentials, leading to low efficiencies of 76% VE and 75% EE.

An examination of the potential behavior with the various electrolytes (Fig. 3) shows the differences in cell potential obtained with the use of 1 M $FeSO_4$ and 1.5 M $FeCl_3$ electrolytes, with the former giving values higher by about 75–90 mV. The difference in cell voltage is attributed to the open-circuit voltage (OCV) of the cell, which is higher in 1 M $FeSO_4$. The OCV is determined by the two half-cell potentials and the extent of crossover of Fe ions through the membrane. Cycle life results showed larger crossover for the 1.5 M $FeCl_3$ system, determined from lower coulombic efficiency (91% vs. 97% in the 1 M $FeSO_4$ electrolyte), which is in correlation with the potential behavior of the two systems. The difference in cell potential may also be a result of variation in the iron half-cell potential, derived from the stability of the solute iron complex. Whereas increased potential is a result of stabilization of the reduced species (Fe(II)) in relation to the oxidized form (Fe(III)), the opposite holds in the case of decreased potential. Higher cell potential is critical for this system since the standard potential of the cell is relatively low, compared to some other redox systems. In this case, 80 mV is more than 10% of the cell potential, a disadvantage of the $FeCl_3$ system.

Another difference between the 1.5 M and 1 M $FeSO_4$ cells must be explained. In the 1.5 M $FeSO_4$ cell the charging process requires a higher voltage than in the 1 M $FeSO_4$ cell, while both exhibit similar voltages during discharge. For both electrolytes, the cycle was initiated at a very low state of charge, and therefore the difference in charging potential is a result of the high overpotential developed,

Table 2
Cycle-life results, with different iron electrolytes, at 60–65 °C.

Electrolyte code	1.5 M $FeCl_3$	1 M $FeSO_4$	1.5 M $FeSO_4$
Discharge capacity [Ah]	0.720	0.608	0.230
Capacity utilization %	90	N/A	29
QE %	91	97	99
VE %	81	84	76
EE %	74	82	75
Discharge AVG voltage [V]	0.53	0.63	0.58

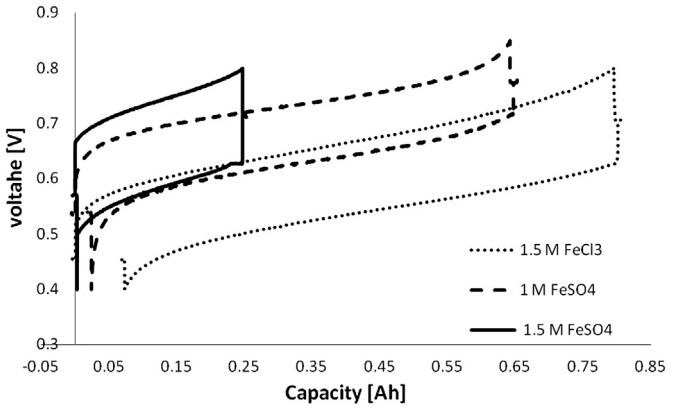

Fig. 3. Cell voltage vs. capacity chart in charge and discharge modes, for different iron electrolytes, taken at 60–65 °C.

in the case of the higher iron concentration. It should be noted that the total overpotential measured on the iron electrode reached a maximum value of 5 mV (at 0.1 A cm^{-2}) for each electrolyte, thus most of the overpotential is developed on the hydrogen electrode. During charging, the hydrogen electrode is negatively charged, attracting migrating iron cations. Increasing the iron concentration at the hydrogen electrode could lead to critical concentration values and even salt precipitation. Indeed, in some 1.5 M $FeSO_4$ cells, at high current-density charging, salt precipitation was observed at the hydrogen electrode. Under these circumstances, mass-transfer processes of protons to the catalytic layer might be hindered, leading to an increase in overpotential during charge. The fact that, in the 1.5 M $FeSO_4$ cell, the discharge step, following charge, shows behavior similar to that of 1 M $FeSO_4$, suggests that the processes disrupting charge, in the case of the higher iron concentration, are fully reversible.

4. Conclusions

The hydrogen/iron cell exhibited high stability with all electrolytes tested, over the testing time frame. The best performance, so far, was achieved with 1 M $FeSO_4$. This electrolyte showed energy-conversion efficiency as high as 82% and a maximal power density of 0.27 W cm^{-2}, with no proper cell optimization. One of the disadvantages of the $FeSO_4$ electrolyte is the difficulty of increasing the iron concentration, as a result of high overpotentials and lower maximal power density. Good results were also obtained with the $FeCl_3$ electrolyte, which may enable increasing iron concentration and therefore, energy density. However, this electrolyte is more corrosive, with a high acid vapor pressure, and so will require the use of more resistant materials which are more costly.

Further research is needed to understand the processes limiting cell performance. Optimization of cell components should increase the power density and efficiencies.

Appendix A. Supplementary material

Supplementary material associated with this article can be found, in the online version, at http://dx.doi.org/doi:10.1016/j.jpowsour.2013.04.032.

References

[1] S. Vazquez, S.M. Lukic, E. Galvan, L.G. Franquelo, J.M. Carrasco, IEEE Trans. Industr. Electron. 57 (12) (Dec. 2010).
[2] C. Ponce de León, A. Frías-Ferrer, J. González-García, D.A. Szánto, F.C. Walsh, J. Power Sources 160 (2006) 716.
[3] A.Z. Weber, M.M. Mench, J.P. Meyers, P.N. Ross, J.T. Gostick, Q. Liu, J. Appl. Electrochem. 41 (2011) 1137–1164.
[4] D.A. Johnson, M.A. Reid, J. Electrochem. Soc. 132 (1985) 1058.
[5] M. López-Atalaya, G. Codina, J.R. Pérez, J.L. Vázquez, A. Aldaz, J. Power Sources 39 (1992) 147.
[6] E. Sum, M. Skyllas-Kazacos, J. Power Sources 15 (1985) 179.
[7] E. Sum, M. Rychcik, M. Skyllas-Kazacos, J. Power Sources 16 (1985) 85.
[8] M. Kazacos, M. Skyllas-Kazacos, J. Electrochem. Soc. 136 (1989) 2759.
[9] M. Skyllas-Kazacos, F. Grossmith, J. Electrochem. Soc. 134 (1987) 2950.
[10] M. Zhang, M. Moore, J.S. Watson, T.A. Zawodzinski, R.M. Counce, J. Electrochem. Soc. 159 (2012) 1183.
[11] T.I. Evans, R.E. White, J. Electrochem. Soc. 134 (1987) 866.
[12] G.D. Simpson, R.E. White, J. Electrochem. Soc. 136 (1989) 2137.
[13] G.D. Simpson, R.E. White, J. Electrochem. Soc. 137 (1990) 1843.
[14] T.I. Evans, R.E. White, J. Electrochem. Soc. 134 (1989) 2725.
[15] K. Fatih, D.P. Wilkinson, F. Moraw, A. Ilicic, F. Girard, Electrochem. Solid-State Lett. 11 (2) (2008) B11–B15.
[16] P. Chen, R.L. McCreery, Anal. Chem. 68 (1996) 3958.
[17] E. Peled, T. Duvdevani, A. Aharon, A. Melman, Electrochem. Solid-State Lett. 3 (12) (2000) 525.
[18] E. Peled, T. Duvdevani, A. Melman, Electrochem. Solid-State Lett. 1 (5) (1998) 210.
[19] C.A. Lucas, N.M. Marković, P.N. Ross, Phys. Rev. B 55 (1997) 7964.
[20] N. Garcia-Araez, V. Climent, P. Rodriguez, J.M. Feliu, Langmuir 26 (14) (2010) 12408.
[21] M. Goor-Dar, N. Travitsky, E. Peled, J. Power Sources 197 (2012) 111.